New Double Many-Body Expansion Potential Energy Surface for Ground-State HCN from a Multiproperty Fit to Accurate ab Initio Energies and Rovibrational Calculations[†]

A. J. C. Varandas* and S. P. J. Rodrigues

Departamento de Química, Universidade de Coimbra 3004-535 Coimbra, Portugal

Received: March 18, 2005

An accurate single-sheeted double many-body expansion potential energy surface has been obtained for the ground electronic state of the hydrogen cyanide molecule via a multiproperty fit to ab initio energies and rovibrational data. This includes 106 rovibrational levels and 2313 discrete points, which are fit with a rmsd of 4 cm^{-1} and 2.42 kcal mol^{-1}, respectively, and seven zero first-derivatives that are reproduced at three stationary points. Since the potential also describes accurately the appropriate asymptotic limits at the various dissociation channels, it is commended both for the simulation of rovibrational spectra and reaction dynamics.

1. Introduction

A few years ago, we reported[1] a global single-valued potential energy surface for the ground electronic state of HCN (heretofore referred to as DMBE I) from a fit to the ab inito data of Bowman et al.[2] using the double many-body expansion[3−5] method. Although an extensive but by no means exhaustive revision of the literature prior to 1995 has then been made,[1] an update may be required since the title system continues to attract much attention due to its prototypical relevance on fundamental issues such as isomerization,[6−9] high-lying vibrational states,[10] potential-energy surface crossings,[11] and quantum chaos.[12] Moreover, the simulation of HCN/HNC[13,14] vibrational−rotational (rovibrational) spectra is of great importance in astrochemistry, particularly in what concerns the detection and assignment of HNC rovibronic levels,[15,16] and the equilibrium constant for the isomerization process HCN ⇌ HNC.[17] It is also well established that HCN plays a key role in the combustion chemistry of nitrogen species,[18,19] where new reaction routes involving this molecule continue to be discussed (see, e.g., ref 20). Furthermore, due to its fundamental importance, several reaction dynamics studies involving HCN have been reported.[21−24]

The most recent potential energy surface for HCN comes from the work of van Mourik et al.,[13] who have based it on a fit to highly accurate ab initio data. Several analytical or semianalytical HCN/HNC potential energy surfaces had, however, been reported previously,[1,2,25−27] some of which by explicitly fitting spectroscopic data.[27−31] Smith et al.[32] have discussed the sensitivity of empirical fits to spectroscopic data, and suggested that the ab initio based potential energy surfaces can be globally better than fully empirical ones. The potentials of Bowman et al.,[2] our previous DMBE I[1] form, and the function of van Mourik et al.[13] have all been modeled along such lines by employing ab initio energies as key data for their calibration.

Starting with an accurate ab initio potential, it seems reasonable to make small corrections to fine-tune the potential such as to achieve spectroscopic accuracy, although the procedure may not be warranted a priori. For example, Wu et al.[31] fitted $J = 0$ and $J = k = 1$ rovibrational data aiming to improve the Bowman et al.[2] potential energy surface for HCN

and found that the final form is a smooth function of the coordinates only when fitting $J = 0$ states alone, becoming nonsmooth when the $J = k = 1$ states are also included. In fact, besides the somewhat straightforward (but often very cumbersome) technical problems that appear when using unrealistic or excessively flexible functions and the subtleties encountered in the experimental data itself, it seems that the inversion problem for polyatomic molecules poses problems of a more fundamental nature. Indeed, it is now consensual that the problem of modeling a polyatomic potential energy surface exclusively from a fit to rovibrational data is generally an undetermined one (i.e., the data can be properly mimicked without leading to the true potential), especially when several minima and barriers are involved. For example, Gadzy and Bowman[28] have shown that it is possible to fit a large set of spectroscopic data for HCN without obtaining a reasonable estimate of the potential barrier for isomerization. Moreover, Carter et al.[30] have reported an empirical potential function from vibrational states of the HCN isomer up to ca. 18 000 cm^{-1} (this is well above the isomerization barrier) that gives reasonable estimates for localized stretching states observed up to 30 000 cm^{-1} [10,33,34] without allowing for the HCN ⇌ HNC isomerization process. Whether the delocalized isomerization states of HCN not yet observed experimentally (see ref 8 for a survey of the literature and a theoretical proposal toward their detection) can lead to a better-posed formulation for the inversion problem based exclusively on spectroscopic data remains therefore an open question.

In the present work, we revisit the issue of obtaining an accurate DMBE model for the potential energy surface of HCN. Our main goal is to slightly improve the long-range functional form reported elsewhere[35] and, following previous work on SO$_2$,[36,37] fit the potential to highly accurate rovibrational data for the HCN[34,38−45] and HNC[46−48] isomers. For this, we employ a multiproperty fit that uses accurate ab initio data[2,13,49] as the starting point. From such a fit, one expects to obtain a globally accurate potential energy surface for HCN/HNC that is shaped by the spectroscopic data in the valence regions associated to the deep minima while being guided there by the ab initio energies, follows the latter at intermediate regions, and is ruled by the best semiempirical estimates of the long-range forces at asymptotic channels.

[†] Part of the special issue "Donald G. Truhlar Festschrift".
* To whom correspondence should be addressed.

Another efficient scheme for including spectroscopic information in potential energy surfaces is the energy switching[35] method. This has been used to obtain local spectroscopic accuracy for several molecular systems, including multisheeted potential energy surfaces.[50−53] Although easy to use, the method relies by its own nature on the quality of the available spectroscopic local potential energy expansions. Although an hybrid approach using an energy switching/fitting methodology may still be employed,[53] its value is yet to be tested on systems such as the title one where subtleties such as the double minimum and isomerization barrier are present.

A final remark to emphasize that the potential energy surface is calibrated from experimental data, and hence it will account implicitly for nonadiabatic and mass-dependent effects. As a result, the final potential energy surface will lie beyond the strict concept that originates from the Born−Oppenheimer approximation, where such effects do not manifest on the potential energy surface. Specifically, we have considered a single isotopomer of the hydrogen cyanid molecule to extract the rovibrational data, namely $^1H^{12}C^{14}N$. Although isotopic mass effects could possibly be better accounted for via a simultaneous fit of the data pertaining to all other isotopomers once weighted according to some scheme, they are likely to be small and possibly within the error of the least-squares fit. Thus, such effects will be heretofore ignored.

The paper is organized as follows. In section 2, we describe the formal representation of the DMBE II potential energy surface, with details of the three-body dispersion, electrostatic, and extended Hartree−Fock (EHF) energies being given in sections 2, 2.1, and 2.2, respectively. Section 3 gives the technical details involved on the least-squares fitting procedure, whereas the main topographical features of the DMBE II potential energy surface are discussed in section 4. The major conclusions are in section 5.

2. Double Many-Body Expansion Potential Energy Surface

Within the DMBE framework,[3−5] a single-sheeted potential energy surface for HCN assumes the form

$$V(\boldsymbol{R}) = \sum_{i=1}^{3}[V_{\text{EHF}}^{(2)}(R_i) + V_{\text{dc},i}^{(2)}(R_i)] + V_{\text{EHF}}^{(3)}(\boldsymbol{R}) + V_{\text{elec}}^{(3)}(\boldsymbol{R}) + V_{\text{dc}}^{(3)}(\boldsymbol{R}) \quad (1)$$

where $V_{\text{EHF},i}^{(n)}$ and $V_{\text{dc},i}^{(n)}$ are the (n = 2 and 3)-body extended Hartree−Fock (EHF) and dynamical correlation terms, and $V_{\text{elec}}^{(3)}$ is the three-body electrostatic energy (note that the electrostatic contributions are absent at two-body level as long as charge overlap effects are ignored). For the two-body terms, we have employed the EHFACE2U[54] potential energy curves reported in ref 1, where the reader is referred for details.

In second-order of perturbation theory, the dynamical correlation energy is mainly due to the long-range dispersion energy which is given by the sum of the pair interactions and hence can be expressed as a sum of inverse powers of the interfragment separation for each channel. For the title system, one may distinguish atom−atom and atom−diatom channels but such a distinction is formal except at the asymptotic limits (note that we are not explicitly accounting for the pure three-body atom−atom-atom contributions which arise in the third-order of long-range perturbation theory). Thus, when the three atoms are well separated, the second-order dispersion energy is given by the
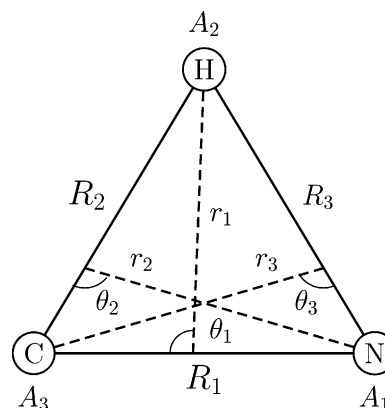
Figure 1. Coordinates used for the HCN/HNC system. The A_i denote parameters with numerical values equal to the atomic masses.

sum of three atom−atom contributions, whereas at each atom−diatom asymptote, it is given by the sum of the atom−diatom intermolecular dispersion interaction plus the intramolecular one. Two approaches have been developed to mimic such a behavior. The first method uses only the knowledge of the atom−atom interaction contributions and interpolates in the remaining of configuration space by considering the united-atoms formed from the coalescing atom−atom and atom−atom−atom interactions at the limit of vanishingly small interatomic distances.[3] An improved scheme to describe the atom−diatom interactions as a function of the intramolecular coordinate has also been reported.[55] As the knowledge of atom−diatom interactions improved, a second approach has been suggested which uses switching forms to allow the switch from the atom−atom to the atom−diatom regimes[35,56] In ref 1, we have used the first approach to construct the HCN DMBE I potential energy surface, whereas in the present work, we adopt the somewhat simpler switching methodology to obtain DMBE II. Thus, we write the three-body dynamical correlation in the form[35]

$$V_{\text{dc}}^{(3)} = -\sum_{i=1}^{3}\sum_{n} f_i(R)C_n^{(i)}(R_i,\theta_i)\chi_n(r_i)r_i^{-n} \quad (2)$$

where i labels the channel A − BC associated with each atom−diatom interaction; R_i is the diatomic internuclear distance, r_i is the separation of atom A from a certain point located in the BC diatomic bond distance, and θ_i is the angle between these two vectors (see Figure 1). In turn, $C_n^{(i)}(R_i,\theta_i)$ are atom−diatom long-range dispersion coefficients to be defined later, and $\chi_n(r_i)$ is the usual dispersion damping functions.[57] Moreover, the three-dimensional switching function assumes the form

$$f_i = \frac{1}{2}\{1 - \tanh[\xi(\eta R_i - R_j - R_k)]\} \quad (3)$$

with the numerical parameters being taken as $\xi = 1\ a_0^{-1}$ and $\eta = 6$. This value has been chosen in order to make the atom−diatom dispersion contributions active only when the diatomic internuclear distances are a factor of 3-fold larger than the mean value of the two other distances. As noted above, there are regions of configuration space where the concept of atom-pair and atom−diatom interactions become ambiguous. To avoid overcounting the dynamical correlation through such terms, we follow our previous approach[35] by switching-off the atom−atom contributions at the atom−diatom limits. Several functional forms have been investigated to represent this switching function, with the best results (judged on a basis of smoothness of the potential energy surface at regions where accurate ab

Potential Energy Surface for Ground-State HCN

J. Phys. Chem. A, Vol. 110, No. 2, 2006 **487**

initio energies are missing) being now obtained by multiplying the two-body dynamical correlation term for the ith pair by $\prod_{j \neq i}(1 - f_j)$.

Following previous work,[36,37] we have chosen to use Jacobi coordinates for the representation of the dynamical correlation, as such coordinates are the most akin to the definition of center of dispersion.[58] This introduces some parameters A_i with values numerically equal to the atomic masses which will then be fixed for all isotopomers of HCN. Thus, no explicit mass-dependence will be introduced on the definition of the potential energy surface. However, as already noted, the final surface implicitly accounts for nonadiabatic and mass effects via the fit to the spectroscopic data, which makes it fall beyond the strict concept that emanates from the Born−Oppenheimer approximation. For the purpose of simplicity, we have also used the approximations[36]

$$r_i = \frac{A_j R_j + A_k R_k}{A_j + A_k} \quad (4)$$

$$\cos \theta_i = \frac{1}{2}\left[\frac{(R_k - R_j)(R_k + R_j)}{R_i} + \frac{A_k - A_j}{A_k + A_j}R_i\right]/r_i \quad (5)$$

Finally, the atom−diatom dispersion coefficients $C_n^{(i)}(R_i,\theta_i)$ of eq 2 assume the form

$$C_n^{(i)}(R_i,\theta_i) = \sum_L C_n(R_i)P_L(\cos \theta_i) \quad (6)$$

where P_L are Legendre polynomials with $L = 0, 2,.., n - 4$ for $n = 6, 8,...,$ and $L = 1, 3,..., n - 4$ for $n = 7, 9, ...$. For homonuclear diatomics, only even anisotropic terms contribute to the dispersion energy expansion. Although odd terms should be considered in constructing the HCN potential energy surface, this will not be done explicitly since the odd leading term is $n = 7$ and hence should not be the dominant one. In turn, the radial dependence of the dispersion coefficients is modeled by the expression[59]

$$C_n^{L,A-BC}(R) = D_M\left(1 + \sum_{i=1}^{3}a_i r^i\right)\exp\left(-\sum_{i=1}^{3}b_i r^i\right) + C_n^{AB} + C_n^{AC} \quad (7)$$

where a_i and b_i are fitting parameters and $r = R - R_M$; $b_1 = a_1$, and R_M is the internuclear distance associated to the position of the maximum in eq 7. All coefficients in eq 7 have been numerically defined elsewhere,[1] and hence will not be given here.

2.1. Electrostatic Energy. The long-range electrostatic potential terms of the HCN system arise from the interaction of the permanent quadrupole moment of the carbon atom with the permanent dipole and quadrupole moments of NH. Following previous work,[1] we describe the electrostatic energy by the form

$$V_{elec} = C_4(R, r)\mathscr{A}_{DQ}(\theta_a,\theta,\phi_{ab})r^{-4} + C_5(R, r)$$
$$\mathscr{A}_{QQ}(\theta_a,\theta,\phi_{ab})r^{-5} \quad (8)$$

where R, r, and θ are the Jacobi coordinates for C−NH interaction, θ_a is the angle that defines the atomic quadrupole orientation, and ϕ_{ab} is the corresponding dihedral angle. Note that the coefficients $C_4(R, r)$ and $C_5(R, r)$ include the associated

charge-overlap damping functions[57]

$$C_4(R, r) = \frac{3}{2}Q_C D_{NH}(R)\tilde{\chi}_4(r)$$

$$C_5(R, r) = \frac{3}{4}Q_C Q_{NH}(R)\tilde{\chi}_5(r) \quad (9)$$

where $D_{NH}(R)$ and $Q_{NH}(R)$ are the permanent electrostatic dipole and quadrupole moments of NH, and Q_C the permanent electrostatic quadrupole moment of the carbon atom. Moreover, the angular functions $\mathscr{A}_{DQ}$ and $\mathscr{A}_{QQ}$ assume the form[60]

$$\mathscr{A}_{DQ}(\theta_a,\theta,\phi_{ab}) = \cos \theta\, (3 \cos^2 \theta_a - 1) + 2 \sin \theta_a \sin \theta \cos \theta_a \cos \phi_{ab} \quad (10)$$

$$\mathscr{A}_{QQ}(\theta_a,\theta,\phi_{ab}) = 1 - 5 \cos^2 \theta_a - 5 \cos^2 \theta + 17 \cos^2 \theta_a \cos^2 \theta + 2 \sin^2 \theta_a \sin^2 \theta \cos^2 \phi_{ab} + 16 \sin \theta_a \sin \theta \cos \theta_a \cos \theta \cos \phi_{ab} \quad (11)$$

Using now the classical-optimized-quadrupole (COQ) model,[1,61−64] the angle θ_a assumes the analytical form[36]

$$\theta_a = \mp\arctan\{2 \sin \theta\, (8C_5 \cos \theta + C_4 R)/ \\ \{[256C_5^2 \sin^2 \theta \cos^2 \theta + \\ 2C_4 C_5 R \cos \theta\, (36 - 25 \sin^2 \theta) + 361C_5^2 \sin^4 \theta + \\ 9C_4^2 R^2 + 144C_5^2]^{1/2} - (5C_4^2 R^2 + 456C_5^2) \sin^2 \theta - \\ 3C_4 R \cos \theta \pm C_5(19 \sin^2 \theta - 12)\}\} \quad (12)$$

As this expression may have singularities on the derivatives at the linear geometries,[65] the angle θ in eq 12 has been scaled to read $\cos \theta \rightarrow \cos \theta'\, (1 - 10^{-4} \cos \theta'^6)$, thus removing such singularities without affecting too much its shape. After substitution of eq 12 into eqs 10, 11, and 8, the analytical COQ model is obtained. The analytical dependence of the CH quadrupole and dipole moments in the internuclear distance are also taken from ref 1.

2.2. Three-Body EHF Energy. The three-body EHF energy is the term that remains after subtracting the sum of the two-body diatomic energies, long-range three-body dispersion, and electrostatic energies from the total potential energy. It is this term that contains the least-squares fitting parameters, being modeled via a distributed n-body approach[66] with $n = 3$

$$V_{EHF}^{(3)} = \sum_{\alpha}P_\alpha(R_1, R_2, R_3)\prod_{i=1}^{3}\{1 - \tanh[\gamma_i^\alpha(R_i - R_{i,\,ref}^\alpha)]\} \quad (13)$$

where each of the $\alpha = 1, 2, 3$ polynomials has the form

$$P_\alpha(R_1, R_2, R_3) = \sum_{ijk}^{i+j+k \leq 5} c_{ijk}^\alpha(R_1 - R_{1,ref}^\alpha)^i(R_2 - R_{2,ref}^\alpha)^j(R_3 - R_{3,ref}^\alpha)^k \quad (14)$$

The complete set of least-squares parameters amounts to 168 c_{ijk}^α linear coefficients and 18 nonlinear ones: 9 γ_i^α, and 9 $R_{i,ref}^{\alpha,\beta}$.

3. Least-Squares Fitting Procedure

The calibration of the EHF term of the DMBE potential energy surface for ground-state HCN has been done by using an automated multiproperty fitting procedure previously em-

488 *J. Phys. Chem. A, Vol. 110, No. 2, 2006*

Varandas and Rodrigues

TABLE 1: Fitted HCN $J = 0$ Vibrational Band Origins Relative to the HCN Zero-Point Energy and Leading Coefficient in Eq 20

N	$(n_1 n_2 n_3)$	calc	exp.	error	$w/10^3$	d_1^2
1	(0 2 0)	1411.39	1411.42	−0.03	1	0.976
2	(1 0 0)	2097.12	2096.85	0.27	1	0.996
3	(0 4 0)	2802.02	2802.96	−0.94	1	0.923
4	(0 0 1)	3313.72	3311.48	2.24	1	0.981
5	(1 2 0)	3502.89	3502.12	0.77	1	0.967
6	(2 0 0)	4173.19	4173.07	0.12	1	0.462
7	(0 6 0)	4172.85	4174.61	−1.76	1	0.540
8	(0 2 1)	4685.96	4684.31	1.65	1	0.896
9	(1 4 0)	4889.30	4888.00	1.30	1	0.902
10	(1 0 1)	5393.69	5393.70	−0.01	1	0.977
11	(0 8 0)	5524.62	5525.81	−1.19	1	0.769
12	(2 2 0)	5571.96	5571.89	0.07	1	0.959
13	(0 4 1)	6039.43	6036.96	2.47	1	0.744
14	(3 0 0)	6228.73	6228.60	0.13	1	0.993
15	(1 6 0)	6256.27	6254.38	1.89	1	0.817
16	(0 0 2)	6520.12	6519.61	0.51	1	0.966
17	(1 2 1)	6759.98	6761.33	−1.35	1	0.881
18	(0 10 0)	6856.81	6855.53	1.28	1	0.687
19	(2 4 0)	6953.28	6951.68	1.60	1	0.883
20	(2 0 1)	7454.37	7455.42	−1.05	1	0.974
21	(3 2 0)	7619.20	7620.22	−1.02	0.01	0.950
22	(0 2 2)	7852.64	7853.51	−0.87	1	0.834
23	(1 4 1)	8109.04	8107.97	1.07	1	0.714
24	(4 0 0)	8264.47	8263.12	1.35	0.01	0.992
25	(2 6 0)	8315.98	8313.53	2.45	0.01	0.785
26	(1 0 2)	8582.70	8585.58	−2.88	1	0.963
27	(2 2 1)	8813.10	8816.00	−2.90	1	0.867
28	(3 4 0)	8994.43	8995.22	−0.79	1	0.863
29	(0 4 2)	9169.21	9166.62	2.59	0.01	0.618
30	(3 0 1)	9496.47	9496.44	0.03	1	0.971
31	(0 0 3)	9625.75	9627.09	−1.34	1	0.954
32	(1 2 2)	9908.81	9914.40	−5.59	0.1	0.820
33	(2 0 2)	10629.18	10631.40	−2.22	0.1	0.960
34	(4 4 0)	11013.30	11015.90	−2.60	0.1	0.843
35	(5 2 0)	11650.48	11654.59	−4.11	0.1	0.937
36	(1 0 3)	11672.21	11674.50	−2.29	0.1	0.951
37	(4 6 0)	12365.79	12364.42	1.37	0.1	0.725
38	(0 0 4)	12641.91	12635.89	6.02	0.1	0.943
39	(3 0 2)	12659.85	12657.88	1.97	0.1	0.957
40	(3 10 0)	13007.93	12999.49	8.44	0.1	0.359
41	(5 4 0)	13011.76	13014.80	−3.04	0.1	0.481
42	(6 2 0)	13635.82	13638.03	−2.21	0.1	0.930
43	(2 0 3)	13707.80	13702.25	5.55	0.1	0.829
44	(5 6 0)	14356.90	14357.05	−0.15	0.1	0.694
45	(4 0 2)	14670.53	14653.66	16.87	0.1	0.951
46	(1 0 4)	14680.15	14670.45	9.70	0.1	0.943
47	(2 2 3)	14979.62	14988.20	−8.58	0.1	0.756
48	(6 4 0)	14986.28	14992.06	−5.78	0.1	0.797
49	(0 0 5)	15581.90	15551.94	29.95	0.1	0.933
	rmsd			5.86		

TABLE 2: Fitted HNC $J = 0$ Vibrational Band Origins Relative to the HNC Zero-Point Energy and Leading Coefficient in Eq 20

N	$(n_1 n_2 n_3)$	calc	exp.	error	$w/10^3$	d_1^2
1	(0 2 0)	926.48	926.51	−0.03	1	0.954
2	(0 4 0)	1873.01	1873.74	−0.73	1	0.884
3	(1 0 0)	2023.65	2023.86	−0.20	1	0.992
4	(1 2 0)	2934.70	2934.82	−0.12	1	0.952
5	(1 4 0)	3868.36	3868.35	0.01	1	0.877
6	(2 0 0)	4027.08	4026.40	0.68	1	0.991
7	(0 0 1)	3651.84	3652.66	−0.82	1	0.965
8	(0 2 1)	4536.00	4534.45	1.55	1	0.841
9	(0 4 1)	5435.81	5435.66	0.14	1	0.656
10	(1 0 1)	5664.55	5664.85	−0.31	1	0.963
11	(0 0 2)	7171.33	7171.41	−0.08	1	0.940
	rmsd			0.62		

TABLE 3: Fitted HCN $J > 0$ Rovibrational Energies Relative to the HCN Zero-Point Energy

N	$(n_1, n_2^l n_3)$	J	calc	exp.	error	$w/10^3$
1	(0 0^0 0)	1	2.96	2.96	0.00	1
2	(0 1^{1e} 0)	1	715.02	714.94	0.09	1
3	(0 1^{1f} 0)	1	715.04	714.95	0.09	1
4	(0 3^{1e} 0)	1	2115.95	2116.41	−0.47	1
5	(0 3^{1f} 0)	1	2115.98	2116.45	−0.47	1
6	(1 0^0 0)	1	2099.97	2099.77	0.20	1
7	(1 1^{1e} 0)	1	2808.81	2808.51	0.29	1
8	(1 1^{1f} 0)	1	2808.82	2808.53	0.29	1
9	(0 0^0 1)	1	3316.70	3314.42	2.28	1
10	(0 5^{1e} 0)	1	3496.58	3498.08	−1.50	1
11	(0 5^{1f} 0)	1	3496.63	3498.13	−1.50	1
12	(0 2^0 0)	1	1414.34	1414.39	−0.05	1
	rmsd				0.93	
1	(0 0^0 0)	2	8.87	8.87	0.00	1
2	(0 1^{1e} 0)	2	720.94	720.85	0.09	1
3	(0 1^{1f} 0)	2	720.98	720.89	0.09	1
4	(0 2^0 0)	2	1420.28	1420.33	−0.04	1
5	(0 2^{2e} 0)	2	1435.33	1435.44	−0.11	1
6	(0 2^{2f} 0)	2	1435.33	1435.44	−0.11	1
7	(0 3^{1e} 0)	2	2121.87	2122.34	−0.47	1
8	(0 3^{1f} 0)	2	2121.97	2122.43	−0.47	1
9	(1 0^0 0)	2	2105.84	2105.55	0.29	1
10	(1 1^{1e} 0)	2	2814.68	2814.31	0.36	1
11	(1 1^{1f} 0)	2	2814.72	2814.36	0.36	1
12	(0 0^0 1)	2	3322.57	3320.24	2.33	1
13	(0 5^{1e} 0)	2	3502.53	3503.95	−1.42	1
14	(0 5^{1f} 0)	2	3502.67	3504.09	−1.42	1
	rmsd				0.86	

SO_2. This is mostly due to the occurrence of two isomers for the title system (HCN and HNC), and to the fact that one requires to calculate vibrational states for values of total angular momentum greater than zero, $J > 0$. All rovibrational calculations have been carried out using the DVR3D and ROTLEV3 suite of programs of Tennyson and co-workers,[67] which employ the two-step approach of Tennyson and Sutcliffe[68] for treating the $J > 0$ case. The Jacobi coordinate option has been utilized with 35 DVR grid points for the H−CN atom−diatom coordinate r, 25 for the CN diatomic coordinate R, and 60 for the angular coordinate θ. Following Harris et al.,[14] the parameters of the Morse oscillator basis have been taken as $R_e = 2.3\ a_0$, $D_e(R) = 29.0\ E_h$, $\omega_e(R) = 0.0105\ E_h$, $r_e = 3.2\ a_0$, $D_e(r) = 5.0\ E_h$, and $\omega_e(r) = 0.004\ E_h$ where the involved coordinates are indicated for clarity (see ref 67 for technical details). An energy cutoff of $-70\,000$ cm^{-1} (the potential minimum is located at $-109\,570$ cm^{-1}) has been used for the 1D solutions, and 1000 2D solutions are used for building the final 3D matrix with dimensions tested over the range 1500−3000. The diagonalization problem has then been solved in the order ($R \rightarrow r \rightarrow \theta$) for obtaining the lowest 200 states. For $J > 0$, 60 states have been calculated from the 200 states obtained in a decoupled

ployed[37] to fit experimental rovibrational data, structural information, and ab initio energies for ground-state SO_2.

The fitted experimental rovibrational data consists of 49 frequencies for HCN ($J = 0$), 11 for HNC ($J = 0$), 12 for HCN ($J = 1$), 9 for HNC ($J = 1$), 14 for HCN ($J = 2$), and 11 for HNC ($J = 2$), in a total of $M = 106$ frequencies taken from Refs. 38−43. For $J = 0$, we have taken the reported band centers, whereas for $J = 1, 2$, the frequencies have been generated with the spectroscopic constants of Maki et al.[42] for HCN and of Maki and Mellau[48] and Northrup et al.[47] for HNC. The l-type splitting of the states with vibrational angular momentum quantum number $l = 1, 2$ has also been taken into account. The fitted levels have been weighted according to the reported experimental error bars, ranging from $w_i = 10$ to 10^3 (see Tables 1−4).

For HCN, the automated assignment of the calculated rovibrational levels raises a more cumbersome problem than the one described elsewhere[37] for the ground electronic state of

Potential Energy Surface for Ground-State HCN

J. Phys. Chem. A, Vol. 110, No. 2, 2006 **489**

TABLE 4: Fitted HNC $J > 0$ Rovibrational Energies Relative to the HNC Zero-Point Energy

N	$(n_1 n_2^l n_3)$	J	calc	exp.	error	$w/10^3$
1	$(0\ 0^0\ 0)$	1	3.02	3.02	0.00	1
2	$(0\ 1^{1e}\ 0)$	1	465.55	465.75	−0.19	1
3	$(0\ 1^{1f}\ 0)$	1	465.57	465.77	−0.20	1
4	$(0\ 2^0\ 0)$	1	929.52	929.55	−0.03	1
5	$(0\ 3^{1e}\ 0)$	1	1403.68	1403.55	0.13	1
6	$(0\ 3^{1f}\ 0)$	1	1403.73	1403.59	0.13	1
7	$(1\ 0^0\ 0)$	1	2026.64	2026.86	−0.22	1
8	$(1\ 1^{1e}\ 0)$	1	2481.28	2481.49	−0.20	1
9	$(1\ 1^{1f}\ 0)$	1	2481.30	2481.51	−0.20	1
	rmsd				0.16	
1	$(0\ 0^0\ 0)$	2	9.07	9.07	0.00	1
2	$(0\ 1^{1e}\ 0)$	2	471.60	471.79	−0.20	1
3	$(0\ 1^{1f}\ 0)$	2	471.66	471.86	−0.20	1
4	$(0\ 2^0\ 0)$	2	935.62	935.65	−0.03	1
5	$(0\ 2^{2e}\ 0)$	2	945.29	945.32	−0.03	1
6	$(0\ 2^{2f}\ 0)$	2	945.29	945.32	−0.03	1
7	$(0\ 3^1\ 0)$	2	1409.76	1409.62	0.14	1
8	$(0\ 3^{1f}\ 0)$	2	1409.88	1409.75	0.13	1
9	$(1\ 0^0\ 0)$	2	2032.64	2032.86	−0.22	1
10	$(1\ 1^{1f}\ 0)$	2	2487.34	2487.55	−0.21	1
11	$(1\ 2^{2f}\ 0)$	2	2953.32	2953.32	0.00	1
	rmsd				0.14	

Coriolis-basis run, where k (the quantum number associated to the projection of J on the z body-fixed axis) is a good quantum number. For the relatively modest number of states needed in our fitting procedure (which extends to ca. 15 500 cm^{-1} above zero-point energy of HCN or ca. 19 000 cm^{-1} above the HCN minimum) it was verified by using larger basis sets and matrix tests that the calculations are converged to within ca. 0.02 cm^{-1}. The expectation values required for the assignment of the frequencies and to calculate the derivatives of the potential with respect to the least-squares parameters based on the Hellmann−Feynman theorem

$$\frac{\partial E_n}{\partial c_k} = \left\langle n \left| \frac{\partial H_{vr}}{\partial dc_k} \right| n \right\rangle = \left\langle n \left| \frac{\partial V(\mathbf{R}:\mathbf{c})}{\partial dc_k} \right| n \right\rangle \quad (15)$$

have been obtained by employing the DVR wave functions generated in the DVR3D code. For $J > 0$, the expansion $\psi_{nJ} = \sum_k C_k \phi_{nJk}$ in terms of the DVR3D solutions ϕ_{nJk} with neglected off-diagonal Coriolis coupling terms is used, with the C_k coefficients being obtained from the ROTLEV3 solutions. Of course, the DVR pivots may differ with the values of k and J but, as $\langle \varphi_{nJk} | \phi_{nJk'} \rangle = \delta_{kk'}$, one gets for the expectation value of an operator $\hat{A}$

$$\langle A \rangle_{nJ} = \sum_k \sum_{\alpha\beta\gamma} (C_k \phi_{nJk}^{\alpha\beta\gamma})^2 A_{\alpha\beta\gamma} \quad (16)$$

which reduces to the usual[67] one term expression for $J = 0$ and $k = 0$. For the automated assignment of the vibrational−rotational states of HCN and HNC, we have employed the scheme shown in flow diagram of Figure 2. For each total angular momentum J and parity p $(= e, f)$, the fit starts with the separation of HCN and HNC states using the expectation values $\langle n | \cos \theta | n \rangle$. Then, the vibrational quantum numbers are estimated using the approach of Menou and Leforestier[69]

$$n_i = \frac{d_i}{2} \frac{\langle n | \Delta Q_i^2 | n \rangle}{\langle 0 | \Delta Q_i^2 | 0 \rangle} - \frac{d_i}{2} \quad (17)$$

where $\Delta Q_i^2 = Q_i^2 - \langle Q_i \rangle^2$ ($i = 1-3$) is obtained from the Q_i normal mode eigenvectors, and the degeneracy of the bending ($d_i = 2$) and stretching ($d_i = 1$) modes has been taken into account. The assignment of the vibrational quantum numbers is complemented with a Dunham expansion fit to the calculated
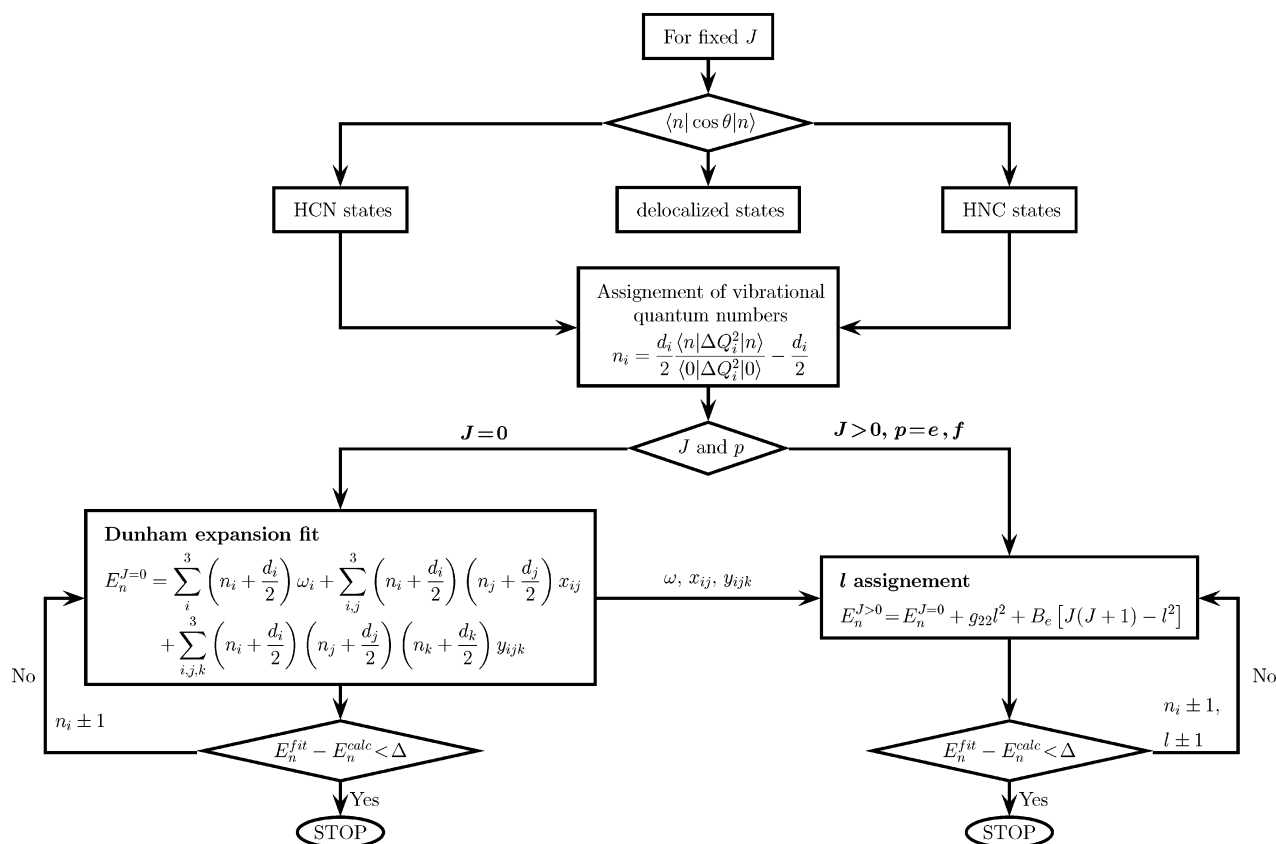
Figure 2. Flowchart of scheme used for automated assignment of states in HCN/HNC.

states similar to the one used in ref 37

$$E_n = \sum_{i=1}^{3}\left(n_i + \frac{d_i}{2}\right)\omega_i + \sum_{i=1}^{3}\sum_{j=1}^{3}\left(n_i+\frac{d_i}{2}\right)\left(n_j+\frac{d_j}{2}\right)x_{ij} +$$
$$\sum_{i=1}^{3}\sum_{j=i}^{3}\sum_{k=j}^{3}\left(n_i+\frac{d_i}{2}\right)\left(n_j+\frac{d_j}{2}\right)\left(n_k+\frac{d_k}{2}\right)y_{ijk} + g_{22}l^2 +$$
$$B_e[J(J+1)-l^2] \quad (18)$$

The vibrational constants ω_i, x_{ij}, and y_{ijk} are fitted to the $J = 0$ calculated vibrational states, and the experimental rotational constants B_e (1.48 and 1.52 cm^{-1} for HCN and HNC) and the vibrational constant g_{22} (5.31 and 3.77 cm^{-1} for HCN and HNC) has been included to account for the rotational and vibrational angular momentum effects on states with $J > 0$. The fit of Dunham expansion has been performed iteratively. This allows the code to correct possible misassignments from eq 17 through the variation of one quanta in the vibrational quantum numbers which appear to be incorrectly assigned within 20 cm^{-1}. The vibrational angular momentum quantum number l is attributed within the course of the fit. The overall numerical procedure is complemented by a visual inspection of selected plots of the wave functions.

The experimental equilibrium geometries of HCN (ref 70) and HNC (ref 71) have also been included in the fit by imposing that the derivatives of the potential energy surface at such geometries should vanish: the corresponding least-squares weights are $w_i = 10^5$. A similar procedure has been used to impose the best ab initio estimate of the saddle-point geometry[13] for the HCN $\rightleftharpoons$ HNC isomerization process, with the associated weight being $w_i = 10^3$. This results in $L = 7$ independent derivatives to fit (note that HCN and HNC have linear structures at equilibrium).

As for the ab initio data, we have included in the fit 256 points CCSD(T) of van Mourik et al.[13] with $w_i = 10$ and 1602 CCSD(T) points of Bowman et al.[2] with $w_i = 1$. These have been chosen from the set of 2172 points reported in ref 2 and have values of the H–CN Jacobi coordinate confined to $r \leq 4$ a_0. All ab initio energies have been scaled linearly such as to reproduce the best estimate of the dissociation energy of HCN obtained by Martin,[49] $\sum D_e = 313.07 \pm 0.25$ kcal mol^{-1} (the value obtained from the fit is $\sum D_e = 313.25$ kcal mol^{-1}). Also included in the least-squares fit, mainly for guiding purposes at regions not covered by the ab initio data and rovibrational frequencies, are 44 scaled FVCAS points[1] obtained for C···H···N regions ($w_i = 0.1$), 627 long-range points ($w_i = 1$) for values of the Jacobi coordinate $r > 5.5$ a_0 (these are obtained as the sum of the two-body diatomic terms and three-body dispersion and electrostatic energies), and 298 short-range points ($w_i = 1$) estimated from the pairwise sum of the three diatomic curves. In addition, we include in the fit the energies of the minima ($w_i = 10^4$) and saddle-point ($w_i = 10^3$) geometries referred to above. All such data resulted in a total of $N = 2830$ energy points to fit, with the final objective function assuming the form

$$F = \sum_{i=1}^{N} w_i(V_i - V_i^{ab})^2 + \sum_{j=1}^{L} w_j\left(\frac{dV_j}{d\mathbf{R}}\right)^2 +$$
$$\sum_{n=1}^{M} w_n(E_n^{calc} - E_n^{exp})^2 \quad (19)$$

A strategy that we found convenient has been to initiate the multiproperty fit with the parameters that are obtained in a fit without including rovibrational data. Using such a scheme and

TABLE 5: Numerical Values of the Extended Hartree–Fock Energy (Eq 13) in Atomic Units

$\gamma_i^\alpha = 1.0$ ($i = 1,2,3; \alpha = 1,2,3$)		
$R_{1,ref}^1 = 2.179$	$R_{2,ref}^1 = 2.013$	$R_{3,ref}^1 = 4.192$
$R_{1,ref}^2 = 2.209$	$R_{2,ref}^2 = 4.087$	$R_{3,ref}^2 = 1.878$
$R_{1,ref}^3 = 2.2439$	$R_{2,ref}^2 = 2.2365$	$R_{3,ref}^2 = 2.6252$
$c_1 = 10.92614897$	$c_2 = -2.15094369$	$c_3 = 4.66712639$
$c_4 = -0.93355317$	$c_5 = 0.07388937$	$c_6 = -0.00581373$
$c_7 = 1.79552186$	$c_8 = 0.42307198$	$c_9 = 0.65109812$
$c_{10} = 0.22250188$	$c_{11} = -0.00450556$	$c_{12} = 3.20875763$
$c_{13} = -1.10809665$	$c_{14} = 1.38008740$	$c_{15} = -0.73826492$
$c_{16} = -0.00240126$	$c_{17} = -0.00851555$	$c_{18} = 0.14413940$
$c_{19} = -0.12772900$	$c_{20} = -0.08111239$	$c_{21} = 0.01635428$
$c_{22} = -2.64618793$	$c_{23} = 0.07188256$	$c_{24} = -1.10077986$
$c_{25} = 0.03490019$	$c_{26} = 0.02981174$	$c_{27} = -1.24185388$
$c_{28} = 0.37584994$	$c_{29} = -0.64015096$	$c_{30} = 0.16136704$
$c_{31} = -0.54840297$	$c_{32} = 0.43779935$	$c_{33} = -0.53388404$
$c_{34} = -0.05890346$	$c_{35} = 0.52667620$	$c_{36} = -0.12872456$
$c_{37} = 0.37359114$	$c_{38} = -0.53407940$	$c_{39} = 0.12465432$
$c_{40} = -0.32926566$	$c_{41} = 0.50155691$	$c_{42} = -0.27429301$
$c_{43} = 0.11297664$	$c_{44} = 0.33335490$	$c_{45} = -0.19574933$
$c_{46} = -0.00103075$	$c_{47} = -0.51848178$	$c_{48} = 0.16372773$
$c_{49} = -0.07052615$	$c_{50} = -0.38579401$	$c_{51} = -0.24703050$
$c_{52} = -0.26807452$	$c_{53} = 0.02219876$	$c_{54} = -0.15165573$
$c_{55} = 0.27461932$	$c_{56} = 0.01951989$	$c_{57} = -6.32864772$
$c_{58} = 0.00781387$	$c_{59} = -2.01142533$	$c_{60} = 0.03176006$
$c_{61} = 0.05152176$	$c_{62} = -0.03364220$	$c_{63} = 1.36851972$
$c_{64} = 0.51442840$	$c_{65} = 1.06415401$	$c_{66} = 0.26178394$
$c_{67} = 0.08306160$	$c_{68} = -2.99500788$	$c_{69} = -0.05528879$
$c_{70} = -0.93179045$	$c_{71} = -0.09186703$	$c_{72} = 0.58275080$
$c_{73} = 0.18743374$	$c_{74} = 0.50817255$	$c_{75} = -0.20017513$
$c_{76} = 0.03598664$	$c_{77} = -0.00694277$	$c_{78} = 4.92635283$
$c_{79} = 1.21067162$	$c_{80} = 1.63981689$	$c_{81} = 0.07814425$
$c_{82} = -0.26586504$	$c_{83} = 0.08816060$	$c_{84} = 0.28757116$
$c_{85} = 0.04326971$	$c_{86} = 0.08018842$	$c_{87} = 2.01780981$
$c_{88} = 0.36517843$	$c_{89} = 0.50284830$	$c_{90} = 0.20566244$
$c_{91} = 0.17578528$	$c_{92} = 0.04430687$	$c_{93} = -0.88311335$
$c_{94} = -0.07486152$	$c_{95} = -0.18734318$	$c_{96} = -0.04105320$
$c_{97} = -0.14321130$	$c_{98} = -0.07100476$	$c_{99} = -0.14391147$
$c_{100} = -0.44685090$	$c_{101} = 0.11627019$	$c_{102} = -0.24918009$
$c_{103} = -0.17343872$	$c_{104} = -0.15367870$	$c_{105} = -0.27343789$
$c_{106} = 0.03395466$	$c_{107} = -0.01012963$	$c_{108} = 0.00489888$
$c_{109} = 0.04765734$	$c_{110} = -0.02148892$	$c_{111} = 0.03927479$
$c_{112} = 0.02319051$	$c_{113} = -20.28094430$	$c_{114} = -4.83531346$
$c_{115} = -8.69722270$	$c_{116} = -1.74855395$	$c_{117} = -0.17012484$
$c_{118} = 0.05528207$	$c_{119} = 0.68285182$	$c_{120} = -1.16393803$
$c_{121} = 0.21859666$	$c_{122} = -0.53971073$	$c_{123} = -0.12638619$
$c_{124} = -6.79524926$	$c_{125} = 0.26555619$	$c_{126} = -2.01754907$
$c_{127} = 0.27622481$	$c_{128} = -0.05475426$	$c_{129} = -0.54288549$
$c_{130} = 0.06540113$	$c_{131} = -0.07754464$	$c_{132} = -0.35253059$
$c_{133} = -0.01244964$	$c_{134} = 1.37236364$	$c_{135} = 4.93902240$
$c_{136} = 1.54088197$	$c_{137} = 1.49631455$	$c_{138} = 0.30000322$
$c_{139} = 1.28142249$	$c_{140} = 0.06097499$	$c_{141} = 1.12939032$
$c_{142} = -0.16077004$	$c_{143} = -1.06598809$	$c_{144} = 1.38282044$
$c_{145} = -0.30676711$	$c_{146} = -0.57184746$	$c_{147} = 0.50451405$
$c_{148} = -0.22761979$	$c_{149} = -4.21417556$	$c_{150} = 0.31848256$
$c_{151} = -1.33584846$	$c_{152} = 0.24505559$	$c_{153} = -0.18571813$
$c_{154} = -1.84014685$	$c_{155} = -0.34292371$	$c_{156} = -0.25393482$
$c_{157} = -0.72723840$	$c_{158} = 0.32476573$	$c_{159} = 1.14785452$
$c_{160} = 0.87062710$	$c_{161} = 0.69087461$	$c_{162} = 0.07850074$
$c_{163} = 0.37538358$	$c_{164} = 0.44975720$	$c_{165} = -0.32247933$
$c_{166} = 0.02015619$	$c_{167} = -0.32098648$	$c_{168} = 0.10629444$

the LMDER routine of MINPACK[72] package which is based on an improved version of the Levenberg-Marquardt method,[73] the convergence is typically reached in 10 iterations (the actual number in the final calculation has been 11). As in previous work,[1,37] the nonlinear parameters of the potential energy surface (γ_i^α and $R_{i,ref}^\alpha$) have been optimized by trial-and-error, being kept fixed in the global fitting procedure. In the present case, the initial estimates appeared to be acceptable, and no further optimization was deemed to be necessary. The final numerical values of the coefficients in the three-body extended-Hartree–Fock energy expression (eq 13) are given in Table 5.

Potential Energy Surface for Ground-State HCN

J. Phys. Chem. A, Vol. 110, No. 2, 2006 **491**
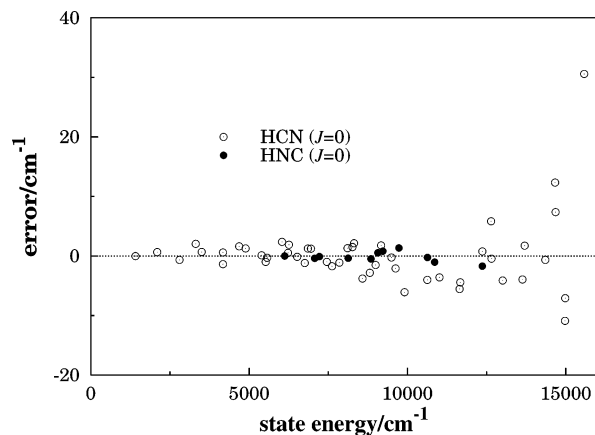
Figure 3. Errors between the experimental and fitted pure vibrational energies of HCN and HNC.
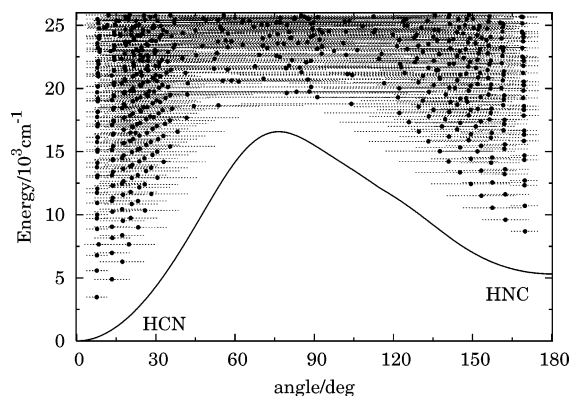

Figure 4. Minimum-energy path for isomerization, HCN ⇌ HNC. Also indicated are the vibrational states of HCN/HNC.

TABLE 6: Stratified Root-Mean-Squared Deviations between the Energy Points and the Analytical DMBE Potential for HCN

points	energy (kcal mol^{-1})	rmsd (kcal mol^{-1})
59	20.0	0.81
243	40.0	1.01
561	60.0	1.25
891	80.0	1.48
1148	100.0	1.70
1377	120.0	1.86
2313	200.0	2.42

In Tables 1−4, we summarize the errors obtained in the fitted rovibrational data, while a graphical view of the errors obtained for the pure vibrational states is shown in Figure 3. In turn, Table 6 collects the errors associated to the fitted ab initio energies. It is seen that they are typically smaller than about 1 up to 40 kcal mol^{-1} above the absolute minimum of the potential energy surface, growing to around 2 kcal mol^{-1} for the total of 2313 points below 200 kcal mol^{-1}.

A graphical display of the positions of the HCN/HNC calculated vibrational states, together with the minimum-energy path of the final potential energy surface for the HCN ⇌ HNC isomerization process is shown in Figure 4. Note that the expectation value $\langle \theta \rangle$ defines the location of each state as a point, while the line defines its uncertainty as $\langle \theta^2 \rangle - \langle \theta \rangle^2$. Note especially the many delocalized states that lie above the barrier (shown by the solid line), which poses an intricate problem to their assignment and hence to their use for obtaining the potential energy surface by inversion of the spectroscopic data. An useful method for characterizing vibrational states is the natural expansion analysis.[74−77] Using this methodology, the
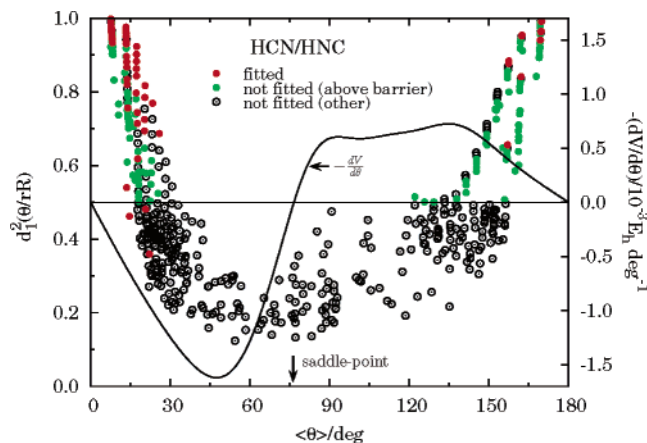
Figure 5. First coefficient ($d_1{}^2$) of the natural expansion as a function of the expectation value of the angular coordinate ($\langle \theta \rangle$) for all calculated $J = 0$ states. Also shown is the angular component of the gradient along the minimum energy path, $-\mathrm{d}V/\mathrm{d}\theta$.

wave function for each state n is expanded as a product of functions, namely

$$\psi_n(r, R, \theta) = \sum_q d_q F_q(\theta) G(r, R) \qquad (20)$$

when the θ coordinate is singled out, with equivalent expansions holding for the r and R coordinates. Within the DVR approximation, $\{d_q{}^2\}$ and $\{F_q\}$ are, respectively, the eigenvalues and eigenvectors of the matrix

$$A_{\gamma'\gamma} = \sum_\alpha \sum_\beta \psi_n^{\alpha\beta\gamma} \, \psi_n^{\alpha\beta\gamma'} \qquad (21)$$

where $\psi_n^{\alpha\beta\gamma}$ are the values of the wave function at the (r_α, R_β, θ_γ) DVR set of points corresponding to the coordinates (r, R, θ); see also ref 78. As it is well established,[74−77] the result $d_1 > 1/2$ implies a dominant function in the natural expansion and indicates that the coordinate is essentially uncoupled from the other two. Values of $d_1{}^2$ for the θ natural expansion obtained for the calculated $J = 0$ states are given (for the fitted levels) in the last columns of Tables 1 and 2 and shown graphically as a function of the vibrationally averaged angle ($\langle \theta \rangle$) for all calculated states in Figure 5. [A full list of the numerical data can be obtained from the authors upon request.] Clearly, the nonlocalized states reported in Figure 4 correspond to those lying below the reference line of $d_1{}^2 < 0.5$. Note that a few such states lie close to the borderline, corresponding to nearly separable states at an average angular geometry in the vicinity of the transition state (this is indicated by the arrow). Note further that most such states lie close to inflection points (or points with a small angular curvature) along the minimum energy path for isomerization, as shown by the solid line ($-\mathrm{d}V/\mathrm{d}\theta$) in Figure 5. Also indicated are the fitted energies which correspond as expected to well localized states. Recall that the nonassigned levels (which are possibly observable[8]) correspond to the majority of the calculated ro-vibrational energies and cannot obviously be fitted by the current approach. However, since the energies of the assigned levels are mimicked with a good accuracy, one may expect those of the unassigned states to offer reliable clues to experimental observation.

4. Features of the Potential Energy Surface

Table 7 provides an exhaustive list of the minima and saddle-points of index 1 existing on the DMBE potential energy surface

TABLE 7: Stationary Points of DMBEII Potential Energy Surface[a]

	R_1/a_0	R_2/a_0	R_3/a_0	E/E_h	ΔE	ω_1	ω_2	ω_3
HCN	2.179	2.013	4.192	−0.4992	313.3[b]	3447.88	729.01	2128.26
	(2.179)[c]	(2.013)[c]	(4.192)[c]		(313.07±0.25)[d]	(3343.1)[e]	(727.0)[e]	(2127.4)[e]
HNC	2.209	4.087	1.878	−0.4750	15.08	3813.71	462.50	2056.98
	(2.209)[f]	(4.087)[f]	(1.878)[f]		(14.8±1.0)[g]	(3813.4, 3816.6)[h]	(460.5, 468.2)[h]	(2059.1, 2059.9)[h]
CNH[†]	2.244	2.237	2.625	−0.4237	48.09	2926.92	1193.01i	2032.51
	(2.258)[i]	(2.241)[i]	(2.634)[i]		(48.4±1.0)[g]			
TS2	4.830	2.863	1.967	−0.1165		4237.42	1092.42i	180.88
TS3	5.620	3.508	2.112	−0.1152		2713.89	235.15	298.47i
TS4	6.080	2.759	3.321	−0.0640		2109.52i	650.41	650.54

[a] Harmonic frequencies are in cm^{-1} and ΔE in kcal mol^{-1}. Experimental and other theoretical values are presented in parentheses. [b] Atomization energy. [c] Experimental geometry (see ref 70). [d] Atomization energy best estimate (see ref 49). [e] Experimental harmonic frequencies (see refs 42. [f] Experimental geometry from ref 71. [g] Theoretical estimate (see ref 80). [h] Experimental harmonic frequencies (see refs 47 and 48). [i] Theoretical estimate (see ref 2).
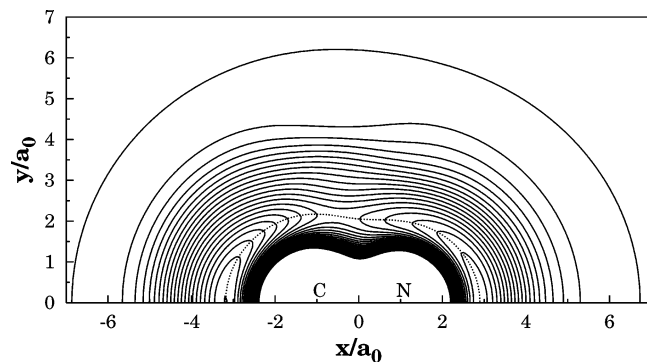
Figure 6. Contour plot for a hydrogen atom moving around a partially relaxed CN diatomic. Contours start at $E_{min} = -0.499E_h$ with $\Delta E = 0.01E_h$.
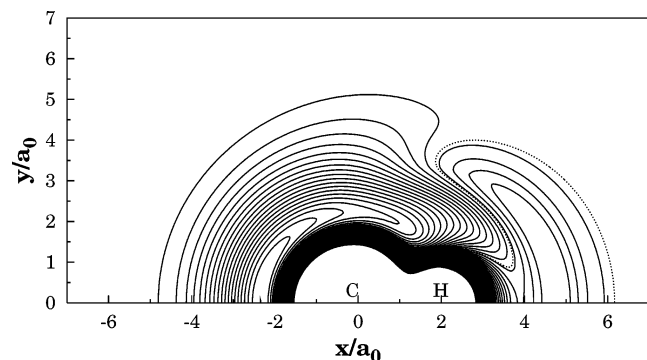

Figure 7. Contour plot for a nitrogen atom moving around a partially relaxed CH diatomic. Contours start at $E_{min} = -0.499E_h$ with $\Delta E = 0.02E_h$.
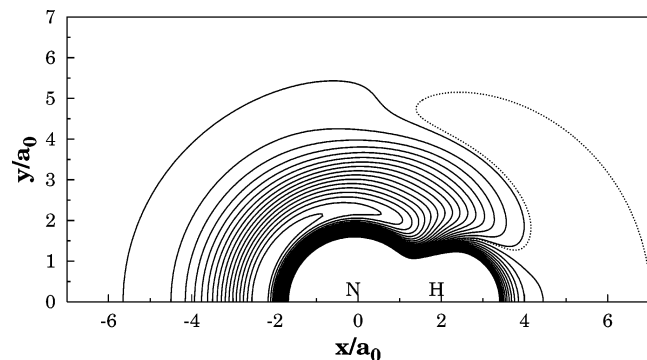
Figure 8. Contour plot for a carbon atom moving around a partially relaxed NH diatomic. Contours start at $E_{min} = -0.499E_h$ with $\Delta E = 0.02E_h$.

(hereafter referred to as DMBE II) obtained in the present work. The global HCN and local HNC appear to be the only minima.
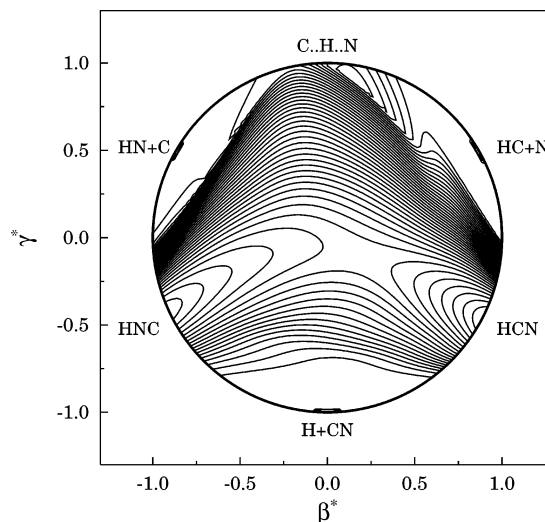
Figure 9. Relaxed triangular plot[79] in hyperspherical coordinates. Contours start at $E_{min} = -0.499E_h$ with $\Delta E = 0.01E_h$.

The most important saddle-point is the CNH[†] that connects those two minima. Other two first-order saddle-points have been detected for weakly bound regions associated to C···H···N structures, but they do not appear to play an important role in the chemistry of the title system as they lie above all atom−diatom asymptotes.

All the major topographical features of the potential energy surface can be seen in Figures 6−8 which present contour plots for an hydrogen atom moving around a partially relaxed CN radical ($2.1144 \leq R_{CN}/a_0 \leq 2.3144$), a nitrogen atom moving around a partially relaxed CH molecule ($1.953 \leq R_{NH}/a_0 \leq 2.153$), and a carbon atom moving around a partially relaxed NH radical ($1.865 \leq R_{NH}/a_0 \leq 2.065$). In Figure 6 are visible the HCN and HNC minima, as well as the saddle-point CNH[†] that connects them. The minimum energy path is indicated by a dashed line. In turn, Figure 7 shows the HCN minimum and regions associated to CH···N structures, whereas in Figure 8 are visible the HNC minimum and NH···C regions. Note that the atom−diatom dissociation energy is indicated by a dashed contour in the last two plots. A global view of the potential energy surface is shown in Figure 9 using a relaxed triangular plot[79] in hyperspherical coordinates.

5. Conclusions

We have obtained a single-valued double many-body expansion (DMBE II) potential energy surface for the ground electronic state of the hydrogen cyanide molecule (HCN) from a multiproperty fit to ab initio energies and spectroscopic rovibrational data. The new surface should be valuable for

Potential Energy Surface for Ground-State HCN

J. Phys. Chem. A, Vol. 110, No. 2, 2006 **493**

studying the HCN/HNC spectra up to very high energies, particularly in what concerns spectra simulation and evolution of the delocalized isomerization states or localized stretching states above the barrier for isomerization. Naturally, it would be interesting to search for regular patterns among the nonassigned levels. In fact, one wonders whether some of the unassigned levels may be attributed to the transition state structure and define accordingly a spectroscopy of the transition state. Work along this direction is currently in progress. Since the DMBE surface of the present work is globally accurate, it can also be useful to calculate the vibrational states of HCN/HNC up to dissociation. Finally, as the dissociation channels are correctly described, it can be used for reaction dynamics studies.

References and Notes

(1) Varandas, A. J. C.; Rodrigues, S. P. J. *J. Chem. Phys.* **1997**, *106*, 9647.

(2) Bowman, J.; Gadzy, B.; Bentley, J.; Lee, T. J.; Dateo, C. E. *J. Phys. Chem.* **1993**, *99*, 308.

(3) Varandas, A. J. C. *Adv. Chem. Phys.* **1988**, *74*, 255.

(4) Varandas, A. J. C. In *Lecture Notes in Chemistry*; Laganá, A., Riganelli, A., Eds.; Springer: Berlin, 2000; Vol. 75, 33.

(5) Varandas, A. J. C. In *Conical Intersections: Electronic Structure, Dynamics and Spectroscopy*; Yarkony, D., Köppel, H., Domcke, W., Eds.; World Scientific Publishing: Singapore, 2004.

(6) Bowman, J. M.; Gadzy, B. *J. Phys. Chem. A* **1997**, *101*, 6384.

(7) Jakubetz, W.; Lan, B. L. *Chem. Phys.* **1997**, *217*, 375.

(8) Bowman, J. M.; Irle, S.; Morokuma, K.; Wodtke, A. *J. Chem. Phys.* **2001**, *114*, 7923.

(9) Barger, T.; Wodtke, A.; Bowman, J. M. *Astrophys. J.* **2003**, *587*, 841.

(10) Martinez, R. Z.; Lehmann, K. K.; Carter, S. *J. Chem. Phys.* **2004**, *120*, 691.

(11) Varandas, A. J. C.; Voronin, A. I.; Jimeno, P. *J. Chem. Phys.* **1997**, *107*, 10014.

(12) Seidel, L.; Gonzalez-Giralda, C.; Benito, R. M.; Borondo, F. *Int. J. Quantum Chem.* **2002**, *86*, 175.

(13) van Mourik, T.; Harris, G.; Polyansky, O. L.; Tennyson, J.; Csázár, A. G.; Knowles, P. *J. Chem. Phys.* **2001**, *115*, 3706.

(14) Harris, G.; Polyansky, O. L.; Tennyson, J. *Spectrochim. Acta A* **2002**, *58*, 673.

(15) Schilke, P.; Commito, C.; Thorwirth, S. *Astrophys. J.* **2003**, *582*, L101.

(16) Harris, G. J.; Pavlenko, Y. V.; Jones, H. R. A.; Tennyson, J. *Month. Not. R. Astron. Soc.* **2003**, *344*, 1107.

(17) Barber, R. J.; Harris, G.; Tennyson, J. *J. Chem. Phys.* **2002**, *117*, 11239.

(18) Miller, J. A.; Bowman, C. G. *Prog. Energy Combust. Sci.* **1989**, *15*, 287.

(19) Hugues, K. J.; Tomlin, A. S.; Hampartsoumian, E.; Zsély, I. G.; Vári, M. U.; Turányi, T.; Clague, A. R.; Pilling, M. J. *Combust. Flame* **2001**, *124*, 573.

(20) Tomeczek, J.; Gradoń, B. *Combust. Flame* **1998**, *133*, 311.

(21) Botina, J.; Rahman, N. *J. Chem. Phys.* **1995**, *102*, 226.

(22) Bowman, J. M.; Padmavathi, D. A. *Mol. Phys.* **1996**, *88*, 21.

(23) Rodrigues, S. P. J.; Varandas, A. J. C. *J. Phys. Chem. A* **1998**, *102*, 6266.

(24) Rodrigues, S. P. J.; Varandas, A. J. C. *J. Phys. Chem. A* **1999**, *103*, 6366.

(25) Murrell, J. N.; Carter, S.; Varandas, A. J. C. *Mol. Phys.* **1978**, *35*, 1325.

(26) Carter, S.; Mills, I. M.; Murrell, J. N. *J. Mol. Spectrosc.* **1980**, *81*, 110.

(27) Murrell, J. N.; Carter, S.; Halonen, L. O. *Mol. Phys.* **1982**, *93*, 307.

(28) Gadzy, B.; Bowman, J. M. *J. Chem. Phys.* **1991**, *95*, 6309.

(29) McCoy, A. B.; III, E. L. S. *J. Chem. Phys.* **1992**, *97*, 2938.

(30) Carter, S.; Mills, I. M.; Handy, N. C. *J. Chem. Phys.* **1993**, *99*, 4379.

(31) Wu, Q.; Zhang, J. Z. H.; Bowman, J. M. *J. Chem. Phys.* **1997**, *107*, 3602.

(32) Smith, A. M.; Klemperer, L.; Lehmann, K. K. *J. Chem. Phys.* **1991**, *94*, 5040.

(33) Romanini, D.; Lehmann, K. K. *J. Chem. Phys.* **1993**, *99*, 6287.

(34) Romanini, D.; Lehmann, K. K. *J. Chem. Phys.* **1995**, *102*, 633.

(35) Varandas, A. J. C. *J. Chem. Phys.* **1996**, *105*, 3524.

(36) Rodrigues, S. P. J.; Sabín, J. A.; Varandas, A. J. C. *J. Phys. Chem. A* **2002**, *106*, 556.

(37) Varandas, A. J. C.; Rodrigues, S. P. J. *Spectrochim. Acta A* **2002**, *58*, 629.

(38) Choe, J.; Tipon, T.; Kukolich, S. G. *J. Mol. Spectrosc.* **1986**, *117*, 292.

(39) Smith, A. M.; Coy, S. L.; Klemperer, L. *J. Mol. Spectrosc.* **1989**, *134*, 134.

(40) Yang, X.; Rogaski, C. A.; Wodtke, A. M. *J. Opt. Soc. Am. B* **1990**, *7*, 1835.

(41) Maki, A.; Quapp, W.; Klee, S.; Mellau, G. C.; Albert, S. *J. Mol. Spectrosc.* **1996**, *180*, 323.

(42) Maki, A.; Mellau, G. C.; Klee, S.; Winnewisser, M.; Quapp, W. *J. Mol. Spectrosc.* **2000**, *202*, 67.

(43) Lecoutre, M.; Rohart, F.; Huet, T. R.; Maki, A. G. *J. Mol. Spectrosc.* **2000**, *203*, 158.

(44) Maki, A.; Quapp, W.; Klee, S.; Mellau, G. C.; Albert, S. *J. Mol. Spectrosc.* **1997**, *185*, 356.

(45) Quapp, W.; Melnikov, V.; Mellau, G. C. *J. Mol. Spectrosc.* **2002**, *211*, 189.

(46) Burkholder, J. B.; Sinha, A.; Hammer, P. D.; Howard, C. J. *J. Mol. Spectrosc.* **1987**, *126*, 72.

(47) Northrup, F. J.; Bethardy, G. A.; Macdonald, R. G. *J. Mol. Spectrosc.* **1997**, *186*, 349.

(48) Maki, A.; Mellau, G. C. *J. Mol. Spectrosc.* **2001**, *206*, 47.

(49) Martin, J. M. L. *Chem. Phys. Lett.* **1996**, *259*, 679.

(50) Varandas, A. J. C. *J. Chem. Phys.* **1997**, *107*, 867.

(51) Varandas, A. J. C.; Rodrigues, S. P. J.; Gomes, P. A. *J. Chem. Phys. Lett.* **1998**, *297*, 458.

(52) Prosmiti, R.; Polyansky, O. L.; Tennyson, J. *Chem. Phys. Lett.* **1997**, *273*, 107.

(53) Varandas, A. J. C. *J. Chem. Phys.* **2003**, *119*, 2596.

(54) Varandas, A. J. C.; Silva, J. D. *J. Chem. Soc., Faraday Trans.* **1992**, *88*, 941.

(55) Varandas, A. J. C. *Chem. Phys. Lett.* **1992**, *194*, 333.

(56) Brandão, J.; Rio, C. A. *Chem. Phys. Lett.* **2003**, *372*, 866.

(57) Varandas, A. J. C. *Mol. Phys.* **1987**, *60*, 527.

(58) Herman, R. M. *J. Chem. Phys.* **1966**, *44*, 1346.

(59) Varandas, A. J. C.; Rodrigues, S. P. J. *Chem. Phys. Lett.* **1995**, *245*, 66.

(60) Buckingham, A. D. *Adv. Chem. Phys.* **1967**, *12*, 107.

(61) Varandas, A. J. C.; Brandão, J.; Quintales, A. M. *J. Phys. Chem.* **1988**, *92*, 3732.

(62) Varandas, A. J. C. *J. Mol. Struct. (THEOCHEM)* **1988**, *166*, 59.

(63) Varandas, A. J. C.; Pais, A. A. C. C. *Mol. Phys.* **1988**, *65*, 843.

(64) Rodrigues, S. P. J.; Varandas, A. J. C. *Phys. Chem. Chem. Phys.* **2000**, *2*, 435.

(65) Rodrigues, S. P. J.; Varandas, A. J. C. *J. Phys. Chem. A* **2003**, *107*, 5369.

(66) Martınez-Núñez, E.; Varandas, A. J. C. *J. Phys. Chem. A* **2001**, *105*, 5923.

(67) Tennyson, J.; Henderson, J. R.; Fulton, N. G. *Comput. Phys. Commun.* **1995**, *86*, 175.

(68) Tennyson, J.; Sutcliffe, B. T. *Mol. Phys.* **1986**, *58*, 1067.

(69) Menou, M.; Leforestier, C. *Chem. Phys. Lett.* **1994**, *210*, 294.

(70) Carter, S.; Mills, I. M.; Handy, N. C. *J. Chem. Phys.* **1992**, *97*, 1606.

(71) Creswell, R. A.; Robiette, A. G. *Mol. Phys.* **1978**, *36*, 869.

(72) J. J. Moré, B. S. Garbow, and K. E. Hillstrom, Argonne National Laboratory, 1980; MINPACK package can be obtained from http://www.netlib.org/minpack/.

(73) Moré, J. J. In *Numerical Analysis, Lecture Notes in Mathematics, vol. 630*; Watson, G. A., Ed.; Springer-Verlag: Berlin, 1977; p 105.

(74) Moiseyev, N.; Wyatt, R. E. *Chem. Phys. Lett.* **1986**, *132*, 396.

(75) Moiseyev, N.; Schatzberger, R.; Froelich, P.; Goscinski, O. *J. Chem. Phys.* **1985**, *83*, 3924.

(76) Moiseyev, N.; Brown, R. C.; Wyatt, R. E.; Tzidoni, E. *Chem. Phys. Lett.* **1986**, *127*, 37.

(77) Moiseyev, N.; Friesner, R. A.; Wyatt, R. E. *J. Chem. Phys.* **1986**, *85*, 331.

(78) Choi, S. E.; Light, J. C. *J. Chem. Phys.* **1992**, *97*, 7031.

(79) Varandas, A. J. C. *Chem. Phys. Lett.* **1987**, *138*, 455.

(80) Lee, T. J.; Rendell, A. P. *Chem. Phys. Lett.* **1991**, *177*, 491.